Research Article | Open Access

Intelligence & Robotics

Liu *et al. Intell. Robot.* **2026**, *6*(2), 275-90 **DOI:**10.20517/ir.2026.14

Physics-informed reduced-order modeling for real-time control of soft actuators

Shengkai Liu[1], Zihan Li[2], Lisi Liu[1], Shengquan Li[1], Jian Jiao[1]

Keywords:
Dynamic modeling, soft actuators, moment-curvature equation, Lagrangian equation, computational efficiency

Citation: Liu, S.; Li, Z.; Liu, L.; Li, S.; Jiao, J. Physics-informed reduced-order modeling for real-time control of soft actuators. *Intell. Robot.* **2026**, *6*(2), 275-90. https://dx.doi.org/10.20517/ir.2026.14

Received: 13 Feb 2026 **First Decision:** 24 Mar 2026 **Revised:** 8 Apr 2026 **Accepted:** 22 May 2026 **Published:** 15 Jun 2026

Academic Editor: Huaicheng Yan
Copy Editor: Pei-Yun Wang
Production Editor: Pei-Yun Wang

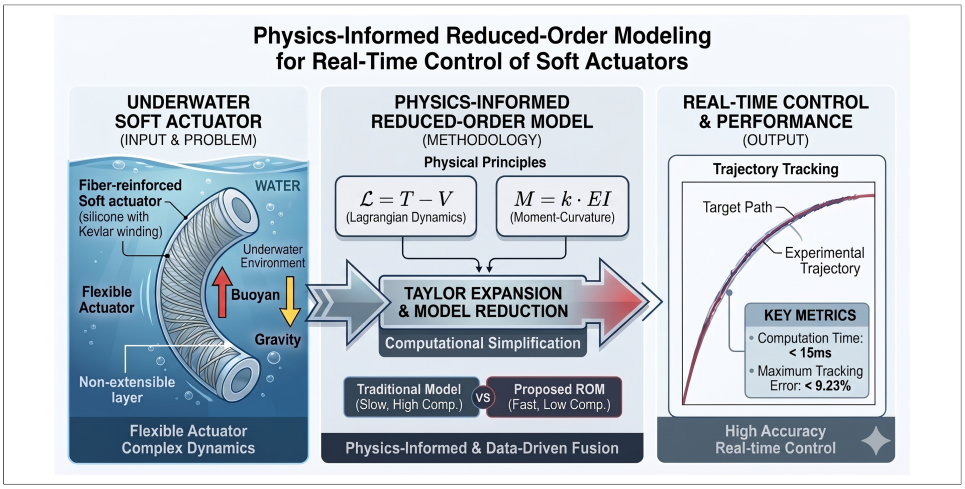

Abstract

The significant deformations and nonlinear characteristics of soft robots pose substantial challenges for accurate modeling. Although various dynamic modeling methods for soft actuators have been explored, existing approaches have excessively long computation times, making them unsuitable for real-time control of soft actuators. To address these issues, this paper proposes an efficient dynamic modeling method for soft actuators. The core idea is to ensure model accuracy by integrating moment-curvature equation with the Lagrangian equation. Additionally, the dynamic model is simplified using Taylor expansion to enhance computational efficiency without compromising control accuracy. The model also accounts for the actuator's gravity and the buoyancy effects of water on its motion. To validate the effectiveness of our proposed model, we performed dynamic model verification experiments in a laboratory setting. The experimental results indicate that the model achieves an error rate of less than 9.23%, with computation times ranging from 0.0094 to 0.015 s. This approach offers a new solution for real-time control of soft actuators.

[1]Peng Cheng Laboratory, Shenzhen 518055, Guangdong, China.
[2]Haikou Experimental Station of the Chinese Academy of Tropical Agricultural Sciences, Haikou 571101, Hainan, China.

Correspondence to: Dr. Jian Jiao, Peng Cheng Laboratory, Shenzhen 518055, Guangdong, China. E-mail: jiaoj01@pcl.ac.cn

1. INTRODUCTION

In recent years, the escalating demand for robotic systems has mirrored the expansion of underwater exploration. However, these environments are inherently complex and dynamic, presenting formidable challenges for conventional rigid robots. Conversely, soft robots, characterized by their intrinsic compliance and safe human–robot interaction capabilities [Figure 1], have emerged as a promising solution[1-3]. To fully realize their potential, developing accurate and computationally efficient dynamic models remains a critical priority[4-6]. Current methodologies generally fall into three categories: data-driven, analytical, and numerical models.

Various data-driven methods have been developed to characterize the dynamic behavior of soft robots. Notably, Braganza *et al.* were among the early researchers to apply neural networks in this domain[7]. By designing a specialized parameter update strategy to replace conventional backpropagation, they developed an approximate model for soft arms. Similarly, Reinhart and Steil introduced a hybrid forward model integrating mechanical principles with learning-based error compensation[8]. This approach significantly enhanced control precision, particularly for the inverse kinematics of redundant soft actuators. Furthermore, Thuruthel *et al.* utilized long short-term memory (LSTM) networks to address long-term dependency issues in sensing signals[9]. Their recurrent architecture enables the simultaneous prediction of position and force in nonlinear, time-varying soft sensors. In a different approach, Holsten *et al.* adopted a direct data-driven method using visual markers to learn three-dimensional kinematics without prior robot knowledge, thereby accommodating manufacturing variations[10]. More recently, Liu *et al.* established a simulation-assisted framework using the SOFA platform to optimize reconfigurable soft grippers[11]. Despite these advancements, such data-driven systems remain computationally intensive during training and often exhibit limited generalization capabilities. While Koopman operator theory provides a means to construct explicit dynamic models, it frequently compromises the precision and bandwidth of the control system[12].

The piecewise constant curvature (PCC) model remains the most prominent analytical approach in soft robotics[13]. This method characterizes the motion of soft actuators by employing idealized geometric and material assumptions to simplify the inherent complexities of continuum mechanics. For instance, Wang *et al.* established a PCC-based kinematic model for an extra-slender dual-stage continuum robot designed for high-precision repair tasks in confined environments[14]. Similarly, Nuelle *et al.* developed a kinematic framework for an active-bending parallel robot, which was subsequently refined via optimization to better align with experimental observations[15]. While these models have been adapted to address certain dynamic issues[16], substantial limitations persist. More advanced frameworks, such as those introduced by Caasenbrood *et al.*[17] and Liu *et al.*[18], utilize the differential geometry of spatial curves to describe nonlinear dynamics and facilitate model-based control. However, a significant drawback of these analytical approaches is their reduced fidelity - and in some cases, total failure - when the actuator is subjected to out-of-plane external forces, most notably gravity.

Modeling soft actuators often presents challenges in obtaining analytical solutions. Existing analytical methods are typically limited to highly idealized conditions, involving simplified geometries, constitutive relations, and boundary conditions. These idealized assumptions diverge significantly from the actual large-scale deformations observed in soft actuators. Consequently, numerical solutions are more prevalent in practical research and applications. Xun *et al.* proposed a nonlinear dynamic model for soft robots based on Cosserat rod theory under the assumption of a piecewise local strain field[19]. The model enables the prediction of dynamic deformations within a general optimization framework during interactions between elongated soft robots and rigid or soft environments. Naughton *et al.* developed an open-source simulation environment called Elastica for simulating the dynamics of soft actuators that can bend, twist, shear, and stretch[20]. By combining Elastica with five state-of-the-art reinforcement learning algorithms, the researchers

Figure 1. Examples of application scenarios.

successfully demonstrated distributed dynamic control of soft robotic arms in various operational scenarios. Ma *et al.* proposed a dynamic model for cable-driven soft tentacles based on Cosserat theory, providing a suite of minimal ordinary differential equation (ODE) models to characterize the relationship between applied tension and bending[21]. Such geometrically exact models have significantly enhanced the accuracy of simulating elongated soft actuators. Furthermore, George Thuruthel *et al.* demonstrated that the high damping and low inertia inherent in soft robots allow for the simplification of dynamic models into first-order equations with negligible accuracy loss, thereby facilitating the development of spatial dynamic controllers[22]. In addition to general frameworks, specialized applications have driven numerical innovation. For instance, Mitros *et al.* introduced a numerical solver for a robotic bronchoscope that markedly improved computational efficiency and deployment capabilities[23]. Alternatively, the finite element method (FEM) serves as a robust tool for capturing complex deformation behaviors. Amehri *et al.* utilized FEM within an optimization-based framework to estimate exterior workspace boundaries while circumventing the high costs of internal configuration calculations[24]. However, these numerical approaches generally suffer from a prohibitive computational load, which frequently precludes their implementation in high-frequency, real-time control loops[25].

In summary, existing modeling methodologies present a clear trade-off between fidelity and efficiency. Purely data-driven modeling methods often suffer from limited generalization due to their opaque black-box nature, which lacks physical interpretability and necessitates exhaustive training datasets. However, traditional analytical models exhibit substantial accuracy degradation under external loads such as gravity, while purely numerical approaches remain computationally prohibitive for real-time control. Therefore, this work proposes an efficient physics-informed reduced-order dynamic modeling framework. We incorporate fundamental physical principles by combining the moment curvature relationship with Lagrangian mechanics, rather than relying purely on data-driven learning. Furthermore, the proposed framework explicitly models environmental forces, including gravity and buoyancy, which are typically neglected in existing Lagrangian-based approaches such as the model presented by Wang *et al.*[26]. This physics-informed formulation improves generalization across varying operating conditions while reducing dependence on large-scale training datasets and preserving physical interpretability. To further address the computational burden associated with conventional dynamic solvers, we employ a Taylor series expansion is employed to simplify the governing equations. The resulting reduced-order formulation significantly improves computational efficiency while retaining the essential system dynamics, thereby enabling real-time control of soft actuators in complex environments.

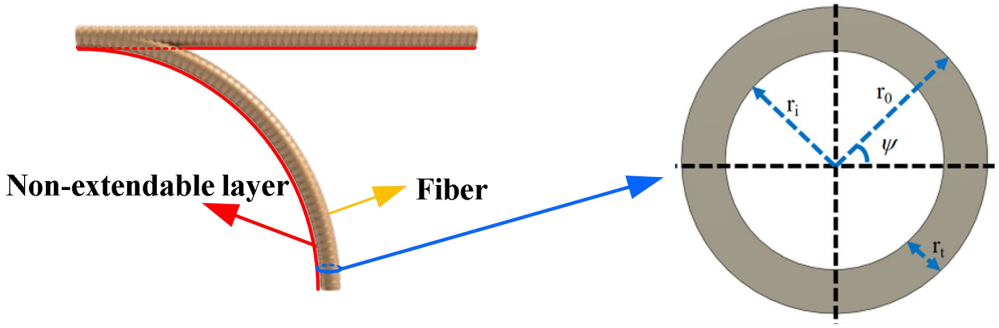

Figure 2. Structural configuration and circular cross-sectional schematic of the soft actuator.

2. GEOMETRIC ANALYSIS AND MODEL DESIGN OF SOFT ACTUATOR

2.1. Geometric analysis

Figure 2 illustrates the structural configuration of the soft actuator used for model validation. The actuator is cast from silicone, and circular surface grooves are subsequently patterned via laser engraving. These grooves enable the integration of Kevlar fibers (DuPont, USA), which reinforce the structure and constrain undesired deformation[27]. An inextensible layer is integrated into the base of the soft actuator to constrain longitudinal expansion during pressurization, thereby enabling localized control over its nonlinear mechanical behavior. Furthermore, to optimize performance, the fiber helix angle should ideally approach 90°.

2.2. Moment-curvature equation

Due to the inherent hyperelasticity of the silicone elastomer, the actuator exhibits pronounced nonlinear deformation behavior. Consequently, the moment-curvature equation is employed to characterize its bending response. The application of internal pressure P generates a resultant thrust force F on the actuator's cross-section. The relationship between the input pressure and the resulting output force is governed by the actuator's geometry.

$$dF = P(r\cos\psi)d(r\sin\psi) = Pr^2\cos^2\psi d\psi \tag{1}$$

where r is the inner radius of the soft actuator and θ is the angle between r and the x-axis. The bending moment M is derived from the resultant moment of the normal stresses σ_x acting over the cross-sectional area S. Accordingly, M is defined as:

$$M = \int_S \sigma_x y dS = \int_0^{2\pi} (r(\sin\psi + 1) + r_t)dF \tag{2}$$

From the fundamental principle of mechanics, the curvature k is proportional to the bending moment M, as expressed in the Euler-Bernoulli framework[28].

$$M = kEI \tag{3}$$

where EI is the flexural rigidity, $R = \frac{1}{k}$ represents the radius of curvature, and $I = \int_A y^2 dS$ denotes the second moment of area. To facilitate the integration with Lagrangian dynamics, Equation (3) is reformulated in terms of the bending angle θ (see Figure 3):

$$k = \frac{1}{R} = \frac{1}{\frac{L}{\theta}} \Rightarrow \theta = \frac{ML}{EI} \tag{4}$$

where L is the effective length of the soft actuator.

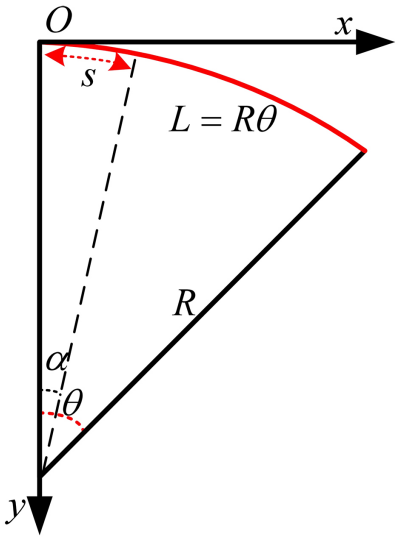

Figure 3. Simplified diagram of the geometry of soft actuators.

To facilitate the formulation of the reduced-order dynamic model, three key physical assumptions are introduced and justified. The first assumption is that the volume of the elastomer remains invariant throughout the deformation process. This is physically grounded in the near-incompressibility inherent to the silicone material used for the soft actuator, which is characterized by a Poisson's ratio of $v \approx 0.5$.

The second assumption is that the deformation of the soft actuator is restricted to a single bending plane. This constraint is kinematically enforced by the structural design; specifically, the embedded Kevlar fibers and the inextensible bottom layer effectively suppress radial expansion and out-of-plane twisting.

The third assumption posits that the soft actuator undergoes constant-curvature deformation. While this geometric approximation is highly effective and physically valid at low-to-moderate actuation pressures, it presents inherent limitations under extreme conditions. Specifically, as the input pressure approaches 90 kPa, the silicone elastomer enters a highly nonlinear hyperelastic regime. Under high-pressure conditions, unmodeled localized phenomena, such as the ballooning effect and minor fiber slippage, may arise, causing the actuator profile to deviate from the ideal constant-curvature assumption. This modeling mismatch constitutes a major source of the increased prediction error observed at elevated pressures. Consequently, the proposed model achieves its highest predictive accuracy within the low-to-moderate pressure operating range.

2.3. Modeling design method

To construct the Lagrangian dynamic model[29] for the soft actuator, it is essential to consider both kinetic energy **T** and potential energy **V**. The primary forms of these energies are as follows:

$$\ell = \mathbf{T} - \mathbf{V} = \mathbf{T} - (S_E + G_P) \tag{5}$$

Where ℓ represents the Lagrangian of the system. S_E and G_P represent strain energy and gravitational potential energy, respectively. By applying the Lagrangian function to the soft actuator, Equation (6) can be derived[26].

$$\frac{d}{dt}\frac{\partial \ell}{\partial \dot{q}_i} - \frac{\partial \ell}{\partial q_i} = Q_i \Leftrightarrow \frac{d}{dt}\frac{\partial \ell}{\partial \dot{\theta}} - \frac{\partial \ell}{\partial \theta} = Q_i \tag{6}$$

Where Q_i denotes a non-conservative generalized force related to P. Based on the principle of virtual work, the generalized force Q_i is derived as:

$$\begin{cases} Q_i = P\frac{\partial V_f(\theta)}{\partial \theta} \\ V_f(\theta) = V_t(\theta) - V_e \end{cases} \tag{7}$$

where $V_f(\theta)$ represents the volume of the internal channels of the soft actuator, $V_t(\theta)$ is the total volume of soft actuators, which can be obtained from Equation (8).

$$\begin{aligned} V_t(\theta) &= \int_0^{\theta} r_o \cos\psi d(\sin\psi) \int_0^{2\pi} (R + r_o + r_o \sin\psi)\, d\alpha \\ &= \int_0^{2\pi}\int_0^{\theta} r_o^2 \cos^2\psi\, (R + r_o + r_o \sin\psi)\, d\alpha d\psi \\ &= \int_0^{2\pi}\int_0^{\theta} r_o^2 \cos^2\psi\, (R + r_o) + r_o^2 \cos^2\psi\, (r_o \sin\psi)\, d\alpha d\psi \\ &= \int_0^{2\pi}\int_0^{\theta} r_o^2 \cos^2\psi\, (R + r_o) + r_o^3 \cos^2\psi (\sin\psi) d\alpha d\psi \\ &= \int_0^{2\pi} r_o^2 \cos^2\psi\, (L + r_o\theta) + \theta r_o^3 \cos^2\psi (\sin\psi) d\psi \\ &= \pi\theta r_o^3 + \pi r_o^2 L \end{aligned} \tag{8}$$

Under the assumption of silicone incompressibility, the elastomer volume V_e remains constant throughout the deformation process and can be expressed by Equation (9).

$$V_e = (\pi r_o^2 - \pi r_i^2)L = \pi L(r_o^2 - r_i^2) \tag{9}$$

The strain energy S_E of soft actuator is determined by integrating the strain energy density U_0 over the elastomer volume V_e. For the silicone elastomer, U_0 is defined using the Neo-Hookean model as $0.5G(I_1 - 3)$, where G is the shear modulus of the soft actuators, I_1 is the first invariant of the Cauchy–Green strain tensor. Given the radial constraints imposed by the fiber reinforcement, we assume $\lambda_2 = 1$ and $\lambda_3 = \frac{1}{\lambda_1}$.

The strain energy of soft actuator S_E can be calculated by the following expression:

$$\begin{aligned} S_E &= \int_{V_e} \tfrac{1}{2} G\,(I_1 - 3)\, dV \\ &= \int_{V_e} \tfrac{1}{2} G \left(\lambda_1^2 + \tfrac{1}{\lambda_1^2} - 2\right) dV \\ &= \int_0^{r_t}\int_0^{2\pi} \tfrac{G}{2} \left(\lambda_1^2 + \tfrac{1}{\lambda_1^2} - 2\right) (r + \tau) L d\psi d\tau \end{aligned} \tag{10}$$

Accordingly, the axial strain λ_1 is determined by the bending angle θ and the associated geometric parameters:

$$\lambda_1 = \left(\frac{((r + \tau)\sin\psi + r)\theta}{R\theta}\right) = 1 + \frac{((r + \tau)\sin\psi + r)\theta}{L} \tag{11}$$

To accurately model the gravitational potential energy in underwater environments, the coupled effects of gravity and buoyancy must be considered. As both the surrounding medium and internal driving fluid are water, the net body force arises from the density difference between the silicone elastomer and the surrounding fluid. Under the assumption of constant actuator volume during deformation, the effective weight is expressed in terms of this density difference, as given in Equation (12).

$$\begin{cases} m_s g = \rho_s V_e g \\ F_f = \rho_w V_e g \end{cases} \Rightarrow mg = \rho_s V_e g - \rho_w V_e g = (\rho_s - \rho_w) V_e g \tag{12}$$

Where m_s, ρ_s represent the mass and density of the soft actuator, g represents gravitational acceleration, F_f and ρ_w represent the buoyancy force and the density of water, respectively. Thus, the calculation method for gravitational potential energy G_p is as follows:

$$G_p = -\frac{mg}{L}\int_0^\theta (R - R\cos\alpha)Rd\alpha = -\frac{mgL}{\theta^2}\int_0^\theta (1-\cos\alpha)d\alpha \tag{13}$$

The tip position of the soft actuator is given by Equation (14).

$$\begin{cases} x(s) = R\sin\theta(s) = R\sin\dfrac{s}{R} \\ y(s) = -R(1-\cos\theta(s)) = R\left(1-\cos\dfrac{s}{R}\right) \end{cases} \tag{14}$$

where s denotes the arc length along the actuator's centerline, and $\theta(s)$ represents the bending angle associated with segment s, as illustrated in Figure 3. Thus, the derived formula for kinetic energy is as follows:

$$\begin{aligned} \mathbf{T} &= \frac{1}{2}mv^2 \\ &= \frac{m}{2L}\int_0^L \left(\frac{dx}{dt}\right)^2 + \left(\frac{dy}{dt}\right)^2 ds \\ &= \int_0^L \left(\frac{dx}{d\theta}\frac{d\theta}{dt}\right)^2 + \frac{m}{2L}\left(\frac{dy}{d\theta}\frac{d\theta}{dt}\right)^2 ds \\ &= mL^2\dot{\theta}^2\left(\frac{1}{6\theta^2} + \frac{1}{\theta^4}(1+\cos\theta) - \frac{2}{\theta^5}\sin\theta\right) \end{aligned} \tag{15}$$

Although all necessary parameters for the dynamic model have been defined, the inherent strong nonlinearity of these equations makes them unsuitable for high-frequency, real-time implementation.

2.4. Solving dynamic models in soft actuator

To improve the computational efficiency of the dynamic model, a Taylor-series-based numerical approximation is employed. The nonlinear terms in the governing equations are truncated at the fifth order to balance modeling accuracy and computational cost. While higher-order terms offer marginal precision gains, they introduce disproportionate calculation burdens that would preclude high-frequency execution. Conversely, the fifth-order truncation effectively preserves the dominant nonlinearities of the system while ensuring the low-latency response required for real-time control applications. The detailed implementation is as follows:

$$\begin{cases} (1+ax)^{-2} = 1 - 2ax + 3(ax)^2 - 4(ax)^3 + \cdots \\ \cos x = 1 - \dfrac{x^2}{2!} + \dfrac{x^4}{4!} - \dfrac{x^6}{6!} + \cdots \\ \sin x = x - \dfrac{x^3}{3!} + \dfrac{x^5}{5!} - \dfrac{x^7}{7!} + \cdots \end{cases} \tag{16}$$

By applying the aforementioned Taylor series expansion, the kinetic energy $\mathbf{T}$, gravitational potential energy G_p, and strain energy S_E are approximated and simplified as follows:

$$\begin{cases} \mathbf{T} \approx \left(\dfrac{1}{40} - \dfrac{\theta^2}{1008}\right)mL^2\left(\dfrac{d\theta}{dt}\right)^2 \\ G_P = -\dfrac{mgL}{\theta^2}\displaystyle\int_0^\theta (1-\cos\alpha)\,d\alpha = -\frac{mgL}{\theta^2}(\theta - \sin\theta) \approx -mgL\left(\frac{\theta}{6} - \frac{\theta^3}{40} + \frac{\theta^5}{5040}\right) \\ S_E \approx \dfrac{2G\theta^2}{L^2}\left(\dfrac{5\pi}{4}r_o^4 - \dfrac{\pi}{4}r_i^4 - \pi r_o^2 r_i^2\right) \\ \dfrac{d}{dt}\dfrac{\partial \ell}{\partial \dot{\theta}} \approx \left(\dfrac{1}{20} - \dfrac{\theta^2}{504}\right)mL^2\dfrac{d^2\theta}{d^2t} - \dfrac{\theta}{252}mL^2\left(\dfrac{d\theta}{dt}\right)^2 \end{cases} \tag{17}$$

The truncation order for the Taylor series expansion was selected to balance mathematical convergence with computational efficiency. Given that the exact nonlinear integrals governing the actuator's system energies lack closed-form analytical solutions suitable for real-time control, the model leverages the rapid convergence of the Taylor series to maintain high-fidelity approximations. At the maximum experimental bending angle (θ_{max} at 90 kPa), the coefficients of the retained terms (e.g., $\frac{1}{5040}$ for θ^5) indicate that subsequent higher-order terms contribute negligibly to the total system energy. Retaining higher-order terms would exponentially increase the computational burden of the ODE45 numerical solver without meaningfully improving precision.

Next, to obtain the numerical solution for Equation (6), we need to establish the boundary conditions.

Boundary Condition 1: As shown in Figure 3, the initial segment of the soft actuator is fixed, so its curvature is zero, $\theta = 0$.

Boundary Condition 2: Assuming no external point load is applied to the distal tip of the soft actuator, the endpoint curvature is primarily governed by the internal pressure-induced moment. Consequently, the curvature at the free end can be directly determined from the input pressure P via the moment-curvature relationship expressed in Equation (4).

By combining the moment–curvature equation with the Lagrangian dynamics formulation, Equation (6) is solved numerically using a shooting method. The resulting nonlinear system is implemented in MATLAB using the built-in functions fsolve and ode45.

The specific computational framework is as follows:
Initial Guess: To initiate the iterative solving process, a strategically selected initial guess is provided to the numerical solver to ensure robust convergence.
Numerical Integration via ODE45: The governing differential equations are numerically integrated using the ode45 solver, starting from the estimated initial parameters across the spatial domain.
Iterative Boundary Matching: The fsolve algorithm is used to iteratively update the unknown initial conditions. The iterations proceed until the integrated terminal states satisfy the prescribed boundary conditions, minimizing the boundary residuals.

3. EXPERIMENTAL

3.1. Determining material parameters for model calibration

Before validating the proposed model, it is necessary to calibrate the material parameters used to fabricate the soft actuator. Previous studies indicate that the material parameters EI of soft actuators are nonlinear, and their values change with variations in input pressure[30,31]. To obtain accurate values for EI, we collected shape and position data of the soft actuators with pressures ranging from 10 to 110 kPa. To facilitate parameter estimation, and given the annular geometry of the soft actuator's cross-section, the second moment of area I is defined as $\pi\left(\frac{r_o^4 - r_i^4}{4}\right)$. Finally, by matching the model's simulation data with the experimental results of the soft actuator, we can derive the fitting formula for how the parameter E of the soft actuator changes with input pressure P.

To calibrate the model under realistic experimental conditions, an input pressure range of 10-110 kPa was defined. The resulting trajectory fitting is illustrated in Figure 4, where M-Trajectory and T-Trajectory denote the predicted deformation and the actual observed data, respectively. Based on these fitting results, the empirical formula characterizing the Young's modulus E of the actuator is formulated as shown in Equation (18).

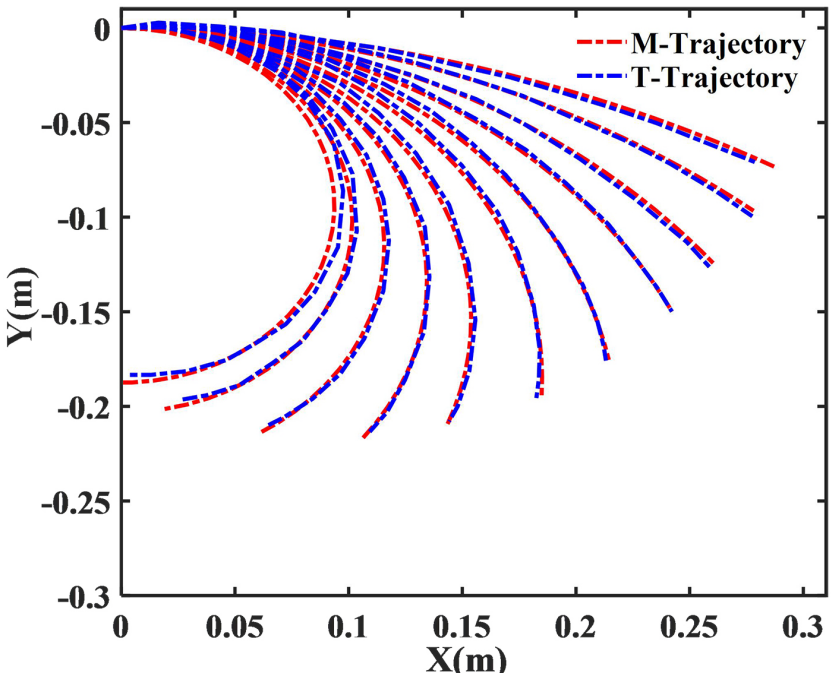

Figure 4. Comparison of simulated and experimental trajectories for the calibration of Young's modulus *E*.

$$E = 1.795 * 10^{-19} * P^5 - 6.36 * 10^{-14} * P^4 + 8.535 * 10^{-9} * P^3 - 5.566 * 10^{-4} * P^2 + 15.97 * P + 6.562 * 10^5 \quad (18)$$

where the unit of Young's modulus E is MPa, the unit of P is Pa.

While physically motivated hyperelastic constitutive models capture the fundamental mechanics of silicone elastomers, their integration into dynamic ODE solvers significantly increases computational cost. As a result, real-time control becomes infeasible. To maximize computational efficiency, an empirical lumped-parameter algebraic mapping was utilized [Equation (18)]. This 5th-order polynomial was calibrated over the 10-110 kPa range, achieving a high goodness-of-fit with an R-squared of 0.9848.

3.2. Validation experiment

To verify the accuracy of the model presented in this study, we selected dynamic data with input pressures ranging from 20 to 90 kPa, as shown in Figure 5. The input form of P is as follows:

$$P = A\sin\left(\frac{2\pi}{T}t\right) \quad (19)$$

where A represents the amplitude of the pressure P, has a range of values between 0 and 90 kPa in the actual experiment, as shown in Figure 5A-D. The pressure is measured using a hydraulic sensor, with data recorded every 0.5 s. T represents the period, and t represents the time. The input pressure control frequency ranges between 0.1 and 0.2 Hz.

The model validation experiment was performed for input pressures ranging from 0 to 20 kPa. Figure 6A and B display the simulated and actual movement trajectories of the soft actuator's end in the x and y directions, respectively. Figure 6C and D present the error rates in these directions, with the experimental data denoted by Exp_{Data} and the model simulation data denoted by M_{Data}. As observed in Figure 6A and B, there is a high degree of overlap between the simulated and experimental trajectories, indicating good agreement between the model and actual performance. To objectively evaluate the effectiveness of the model,

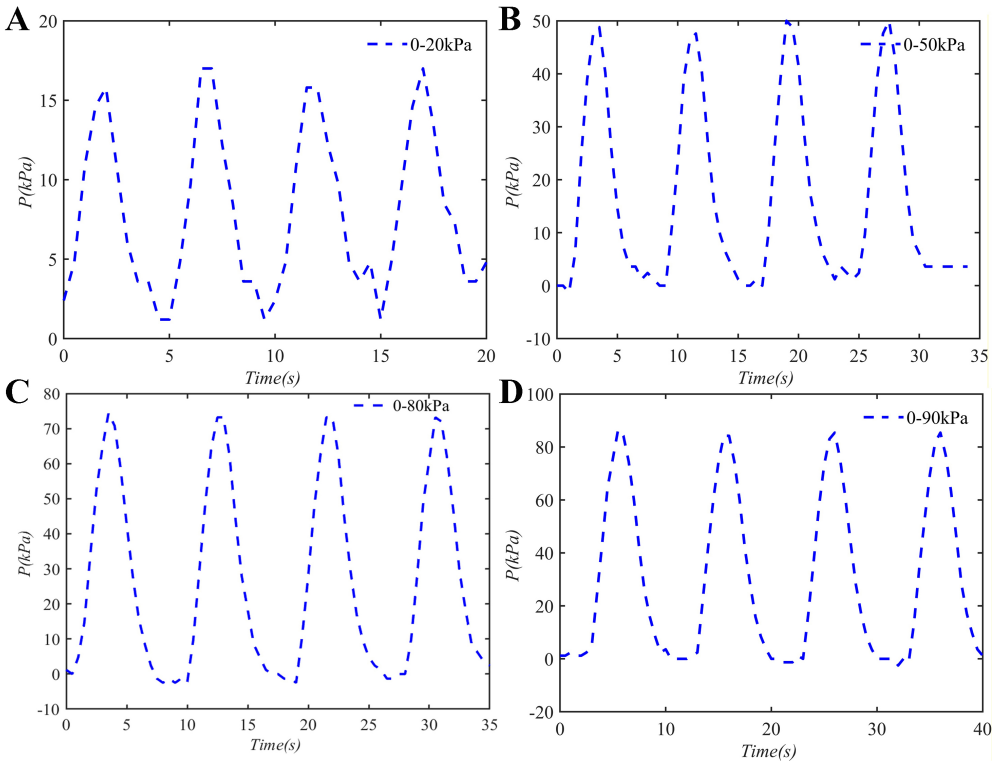

Figure 5. Schematic diagram of pressure variation in the soft actuator.

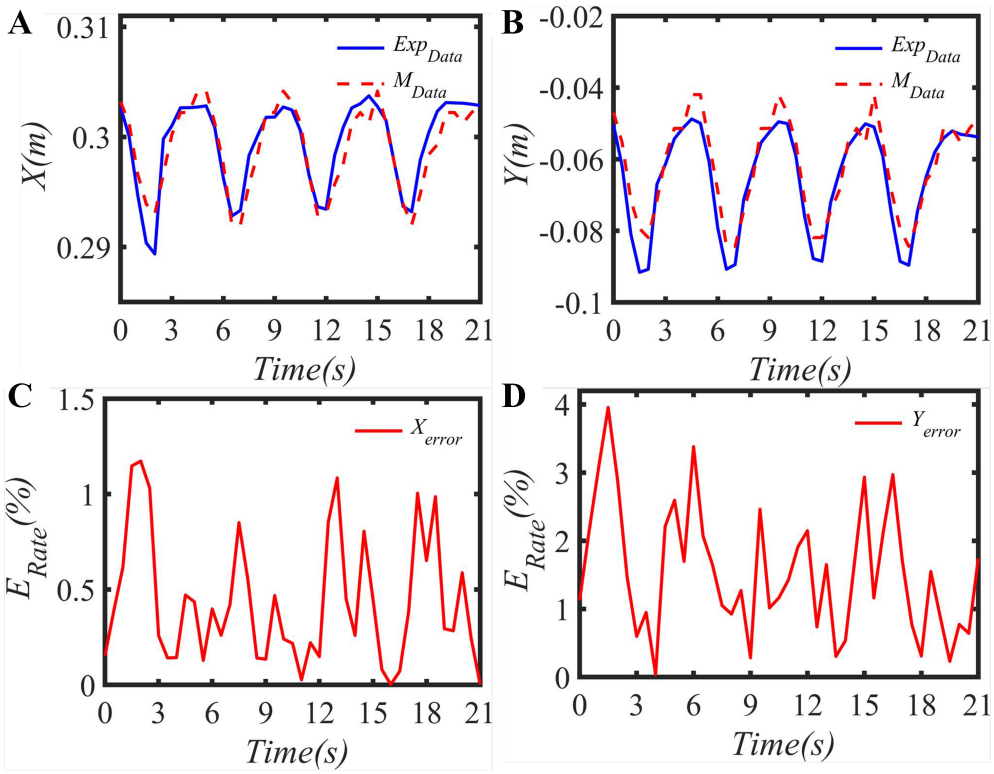

Figure 6. Comparison of model data and experimental data for an input pressure of 0-20 kPa.

we define the error rate E_{Rate} calculation formula as follows:

$$E_{Rate} = \frac{||M_{Date} - Exp_{Data}||}{L} \times 100\% \tag{20}$$

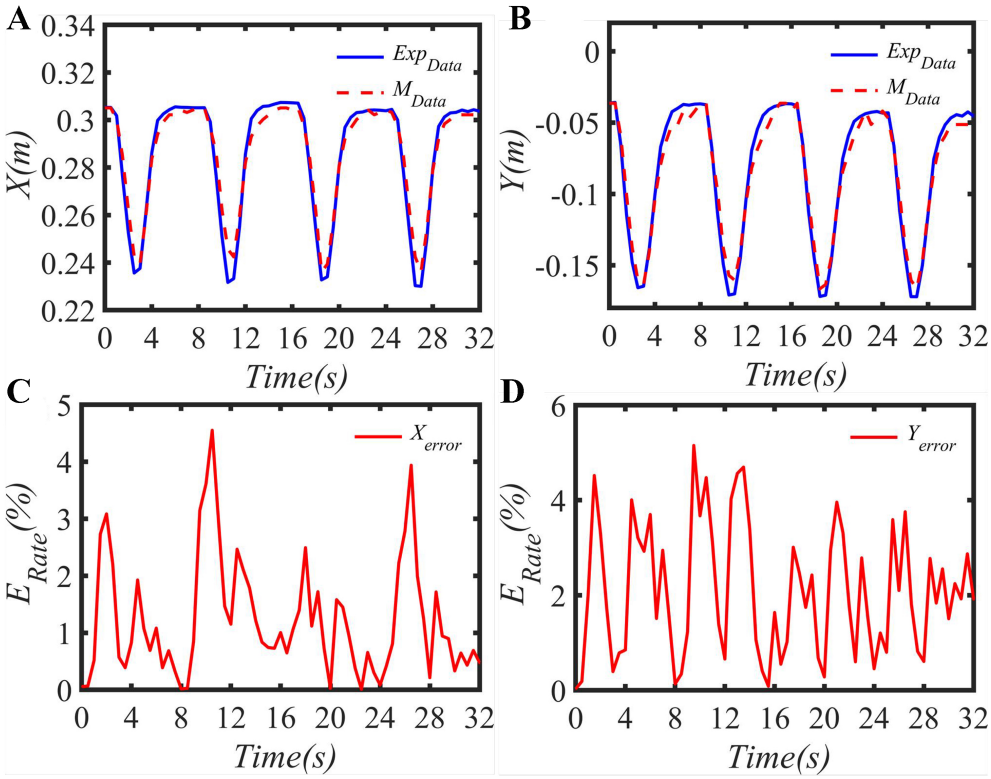

Figure 7. Comparison of model data and experimental data for an input pressure of 0-50 kPa.

The error rates calculated using Equation (20) are shown in Figure 6C and D.

The proposed model demonstrates a maximum relative error rate of less than 1.17% in the x-direction and less than 3.96% in the y-direction, normalized by the total length of the soft actuator. Furthermore, the model achieved a mean computational time of 0.0094 s per step, effectively fulfilling the stringent low-latency requirements for real-time implementation.

In the second validation experiment, the dynamic response of the soft actuator was further evaluated by increasing the pressure amplitude to 50 kPa and adjusting the input frequency. As illustrated in Figure 7A and B, the proposed model exhibits robust tracking fidelity across both the x and y directions. Quantitative results in Figure 7C and D reveal that the peak relative errors are constrained within 4.55% and 5.15% respectively. These findings confirm that the model maintains consistent performance even under elevated input pressures. Furthermore, the mean computational latency per iteration under these conditions was recorded at 0.0127 s.

In the third experiment, the actuation pressure range was extended to 80 kPa, while the pressure control frequency was also appropriately adjusted. Figure 8A and B illustrates the trajectory tracking performance of the soft actuator tip under the above experimental conditions. These figures show the effectiveness of the model in tracking the desired trajectories over the extended pressure range. Furthermore, Figure 8C and D illustrate that the proposed model restricts the peak relative prediction errors for the soft actuator's end trajectory to under 7.08% in the x-direction and 5.99% in the y-direction. Under the experimental condition, the average time required to solve each step is 0.0122 s.

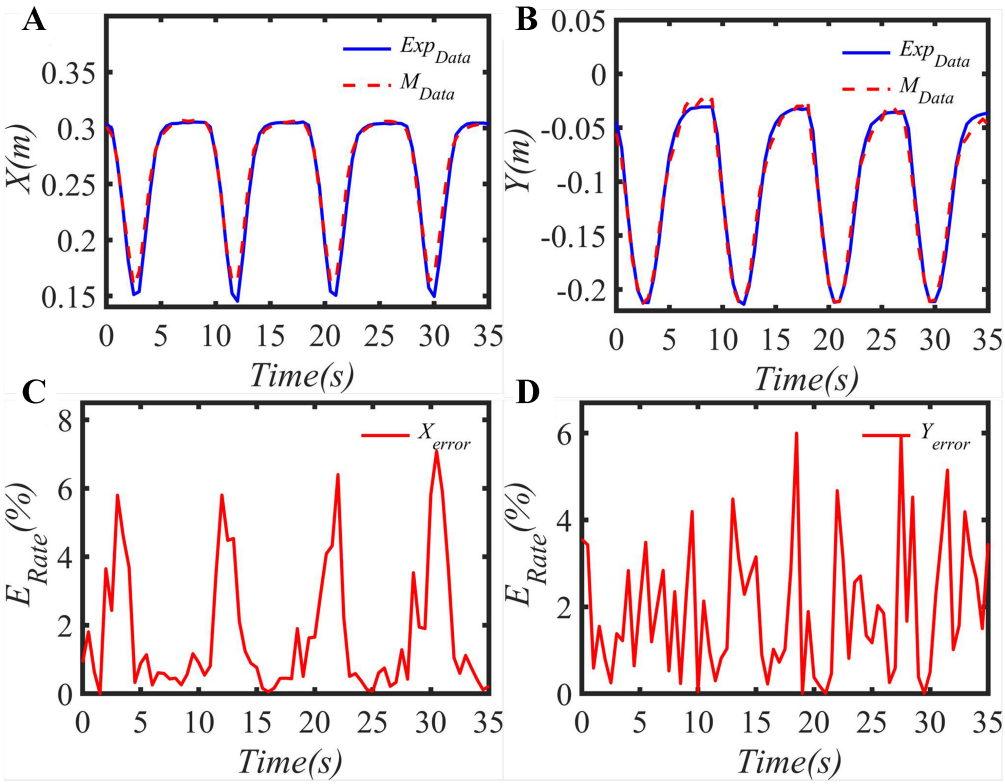

Figure 8. Comparison of model data and experimental data for an input pressure of 0-80 kPa.

In the fourth validation scenario, the input pressure reached 90 kPa to assess the model's robustness under large hyperelastic deformations. The corresponding trajectory tracking results are depicted in Figure 9A and B. Specifically, Figure 9C and D demonstrate that the proposed model maintains a peak relative tracking error of less than 9.23% in the x-direction and 5.88% in the y-direction. Despite the presence of unmodeled local deformations at this pressure level, the results indicate that the model can accurately predict the actuator's spatial trajectory with acceptable error levels. Furthermore, the mean computational latency remained low at 0.015 s per iteration.

In addition to visual comparisons and peak errors, the mean absolute error (MAE) and root mean square error (RMSE) were calculated for both the x and y trajectories across all four validation experiments (20, 50, 80, and 90 kPa). These statistical metrics are summarized in Table 1, providing a clear and objective assessment of the model's tracking reliability.

As indicated by the statistical metrics, the model exhibits excellent tracking accuracy and repeatability under low to moderate pressures (0-80 kPa). However, a noticeable increase in the prediction error is observed at the extreme pressure of 90 kPa, where the peak error reaches 9.23%. This deviation stems from the inherent physical limitations of the assumed kinematic geometry. At lower pressures, the soft actuator undergoes quasi-linear deformation, adhering strictly to the constant-curvature assumption. Conversely, as the internal pressure approaches 90 kPa, the silicone elastomer enters a highly nonlinear hyperelastic regime. Extreme pressurization induces unmodeled local deformations, such as slight radial expansion despite the fiber constraints, as well as visco-elastic hysteresis. These phenomena alter the local stiffness and curvature, causing the actuator's actual shape to deviate from an ideal uniform curvature. Recognizing this physical boundary is crucial, as it defines the optimal and reliable operating range (0-80 kPa) for the proposed physics-informed reduced-order model. Although direct quantitative comparison of tracking errors with

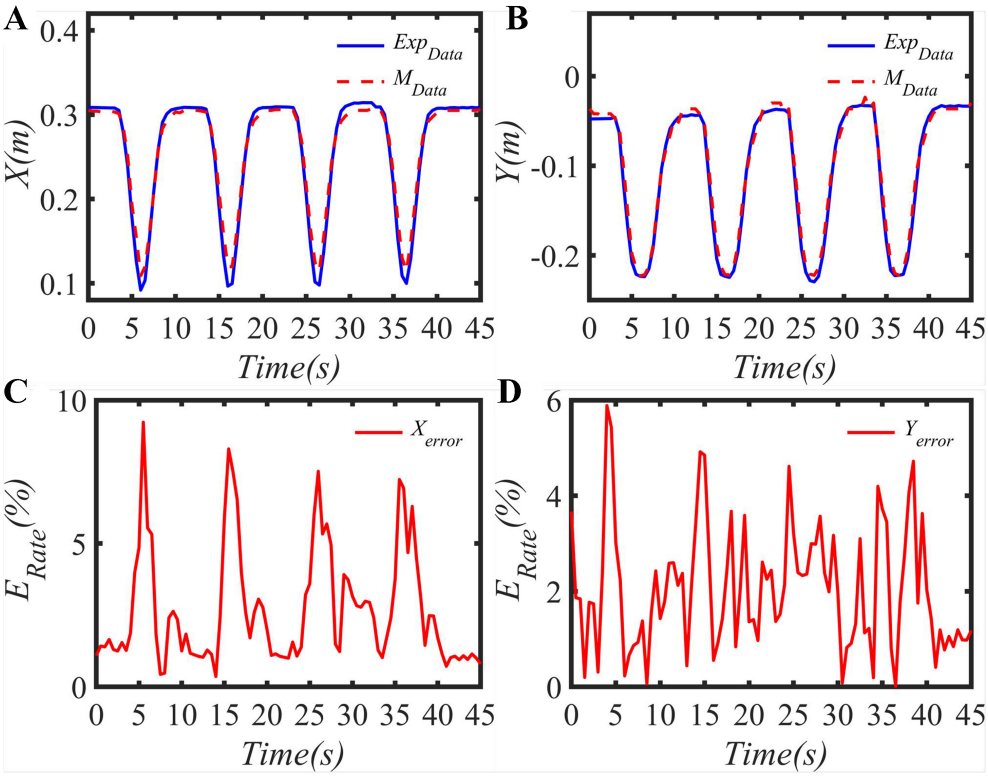

Figure 9. Comparison of model data and experimental data for an input pressure of 0-90 kPa.

Table 1. Statistical tracking errors of the proposed model under varying input pressures

Input pressure (kPa)	X-axis-MAE (m)	X-axis RMSE (m)	Y-axis MAE (m)	Y-axis RMSE (m)
0-20	0.00134	0.00169	0.00475	0.00553
0-50	0.00372	0.00486	0.00646	0.00767
0-80	0.00525	0.00772	0.00599	0.00755
0-90	0.00831	0.0104	0.00633	0.00749

MAE: Mean absolute error; RMSE: root mean square error.

established approaches such as FEM or Cosserat rod models is often hindered by differences in experimental configurations, their computational trade-offs are widely acknowledged in the literature. Purely numerical methodologies, particularly FEM-based frameworks, offer exceptional theoretical fidelity by capturing high-dimensional degrees of freedom; however, their execution times typically range from seconds to minutes per step, confining them to offline design rather than real-time control. Similarly, Cosserat rod models effectively resolve 3D continuum dynamics. However, solving the underlying partial differential equations introduces latency on the order of tens to hundreds of milliseconds, limiting their suitability for high-frequency control loops. Furthermore, even analytical Lagrangian frameworks can encounter computational bottlenecks when integrated with non-linear environmental forces, such as buoyancy and hydrodynamic drag.

In contrast, the physics-informed reduced-order model proposed in this study is specifically optimized to break this computational bottleneck. By utilizing Taylor series expansion to reduce the model's order, the proposed method achieves an extremely efficient execution time of approximately 0.015 s per step. Although this profound simplification results in a bounded peak error of 9.23% under extreme hyperelastic

deformations (90 kPa), it successfully fulfills the stringent low-latency requirements of dynamic closed-loop systems. This establishes a highly pragmatic trade-off, prioritizing extreme computational efficiency while maintaining an operationally acceptable tracking accuracy for soft actuators in complex environments.

4. CONCLUSIONS

To formulate the dynamic relationship between input pressure and soft actuator deformation, this study presents a physics-informed reduced-order modeling framework that integrates the moment-curvature equation with Lagrangian dynamics. Within this framework, Lagrangian dynamics establishes the foundational governing model, while the moment-curvature relationship provides the necessary boundary conditions. To overcome the computational bottlenecks of traditional numerical methods, a Taylor series expansion is implemented to simplify the analytical formulation. This reduction technique significantly enhances computational efficiency without compromising physical fidelity, effectively accounting for complex environmental forces such as gravity and buoyancy.

Comprehensive experimental validations, quantified through statistical metrics (e.g., MAE and RMSE), confirm the model's high tracking precision. The proposed framework exhibits excellent reliability within the 0-80 kPa range and maintains a peak relative error of 9.23% even under extreme hyperelastic deformations at 90 kPa. Furthermore, the model achieves a mean computational time of 0.015 s per iteration, enabling high-frequency, real-time closed-loop control. Future research will focus on implementing this dynamic model in autonomous physical control systems and extending the framework to characterize complex three-dimensional spatial deformations.

DECLARATIONS

Authors' contributions

Concept and design: Liu, S.
Fabrication and method: Jiao, J.; Li, Z.
Modeling and analysis: Liu, S.; Li, S.
Experiment and validation: Liu, S.; Liu, L.
Writing and editing: Liu, S.; Jiao, J.

Availability of data and materials

The data that support the findings of this study are available from the corresponding author upon reasonable request.

AI and AI-assisted tools statement

During the preparation of this manuscript, the AI tool Gemini was used solely for language editing. The tool did not influence the study design, data collection, analysis, interpretation, or the scientific content of the work. All authors take full responsibility for the accuracy, integrity, and final content of the manuscript.

Financial support and sponsorship

This study was supported by the Shenzhen Science and Technology Program (Grant No. RCBS20231211090816033), the Director Foundation Project of PCL (Grant Nos. PCL2025A13, PCL2025A12, and PCL2025A17), and the Guangdong S&T Program under Grant (Grant No. 2024B0101010003).

Conflicts of interest

All authors declared that there are no conflicts of interest.

Ethical approval and consent to participate

Not applicable.

Consent for publication

Not applicable.

REFERENCES

1. Li, J.; Wang, L. Modeling magnetic soft continuum robot in nonuniform magnetic fields via energy minimization. *Int. J. Mech. Sci.* **2024**, *282*, 109688. DOI
2. Kulkarni, M.; Edward, S.; Golecki, T.; Kaehr, B.; Golecki, H. Soft robots built for extreme environments. *Soft. Sci.* **2025**, *5*, 12. DOI
3. Huang, X.; Xiang, H.; Wu, C.; et al. CRAB-EDM: a multi-modal underwater crab-inspired robot with temporally sequenced electro-discharge modulation. *IEEE. Robot. Autom. Lett.* **2026**, *11*, 3939-46. DOI
4. Sun, W.; Liang, H.; Zhang, F.; et al. Dielectric elastomer minimum energy structure with a unidirectional actuation for a soft crawling robot: design, modeling, and kinematic study. *Int. J. Mech. Sci.* **2023**, *238*, 107837. DOI
5. Chen, H.; Ali, M. A.; Wang, Z.; Chen, J.; Ramadan, M. N.; Alkhedher, M. Performance optimizing of pneumatic soft robotic hands using wave-shaped contour actuator. *Results. Eng.* **2025**, *25*, 103456. DOI
6. Zolfagharian, A.; Lakhi, M.; Ranjbar, S.; Tadesse, Y.; Bodaghi, M. 3D printing non-assembly compliant joints for soft robotics. *Results. Eng.* **2022**, *15*, 100558. DOI
7. Braganza, D.; Dawson, D.; Walker, I.; Nath, N. A neural network controller for continuum robots. *IEEE. Trans. Robot.* **2007**, *23*, 1270-7. DOI
8. Reinhart, R. F.; Steil, J. J. Hybrid mechanical and data-driven modeling improves inverse kinematic control of a soft robot. *Procedia. Technol.* **2016**, *26*, 12-9. DOI
9. Thuruthel, T. G.; Shih, B.; Laschi, C.; Tolley, M. T. Soft robot perception using embedded soft sensors and recurrent neural networks. *Sci. Robot.* **2019**, *4*, eaav1488. DOI PubMed
10. Holsten, F.; Engell-Nørregård, M. P.; Darkner, S.; Erleben, K. Data driven inverse kinematics of soft robots using local models. In *2019 International Conference on Robotics and Automation (ICRA)*, Montreal, Canada, May 20-24, 2019. IEEE; 2019. pp. 6251-7. DOI
11. Liu, J.; Low, J. H.; Han, Q. Q.; et al. Simulation data driven design optimization for reconfigurable soft gripper system. *IEEE. Robot. Autom. Lett.* **2022**, *7*, 5803-10. DOI
12. Bruder, D.; Fu, X.; Gillespie, R. B.; Remy, C. D.; Vasudevan, R. Data-driven control of soft robots using Koopman operator theory. *IEEE. Trans. Robot.* **2021**, *37*, 948-61. DOI
13. Della Santina, C.; Bicchi, A.; Rus, D. On an improved state parametrization for soft robots with piecewise constant curvature and its use in model based control. *IEEE. Robot. Autom. Lett.* **2020**, *5*, 1001-8. DOI
14. Wang, M.; Dong, X.; Ba, W.; Mohammad, A.; Axinte, D.; Norton, A. Design, modelling and validation of a novel extra slender continuum robot for *in-situ* inspection and repair in aeroengine. *Robot. Comput. Integr. Manuf.* **2021**, *67*, 102054. DOI
15. Nuelle, K.; Sterneck, T.; Lilge, S.; Xiong, D.; Burgner-Kahrs, J.; Ortmaier, T. Modeling, calibration, and evaluation of a tendon-actuated planar parallel continuum robot. *IEEE. Robot. Autom. Lett.* **2020**, *5*, 5811-8. DOI
16. Falkenhahn, V.; Hildebrandt, A.; Neumann, R.; Sawodny, O. Model-based feedforward position control of constant curvature continuum robots using feedback linearization. In *2015 IEEE International Conference on Robotics and Automation (ICRA)*, Seattle, USA, May 26-30, 2015. IEEE; 2015. pp. 762-7. DOI
17. Caasenbrood, B. J.; Pogromsky, A. Y.; Nijmeijer, H. Dynamic modeling of hyper-elastic soft robots using spatial curves. *IFAC. PapersOnLine.* **2020**, *53*, 9238-43. DOI
18. Liu, S.; Jiao, J.; Meng, F.; Mei, T.; Sun, X.; Kong, W. Modeling of a soft actuator with a semicircular cross section under gravity and external load. *IEEE. Trans. Ind. Electron.* **2023**, *70*, 4952-61. DOI
19. Xun, L.; Zheng, G.; Kruszewski, A. Cosserat-Rod-based dynamic modeling of soft slender robot interacting with environment. *IEEE. Trans. Robot.* **2024**, *40*, 2811-30. DOI
20. Naughton, N.; Sun, J.; Tekinalp, A.; Parthasarathy, T.; Chowdhary, G.; Gazzola, M. Elastica: a compliant mechanics environment for soft robotic control. *IEEE. Robot. Autom. Lett.* **2021**, *6*, 3389-96. DOI
21. Ma, J.; Han, Z.; Yang, L.; Min, G.; Liu, Z.; He, W. Dynamics modeling of a soft arm under the Cosserat theory. In *2021 IEEE International Conference on Real-time Computing and Robotics (RCAR)*, Xining, China, Jul 15-19, 2021. IEEE; 2021. pp. 87-90. DOI
22. George Thuruthel, T.; Renda, F.; Iida, F. First-order dynamic modeling and control of soft robots. *Front. Robot. AI.* **2020**, *7*, 95. DOI PubMed PMC
23. Mitros, Z.; Thamo, B.; Bergeles, C.; da Cruz, L.; Dhaliwal, K.; Khadem, M. Design and modelling of a continuum robot for distal lung sampling in mechanically ventilated patients in critical care. *Front. Robot. AI.* **2021**, *8*, 611866. DOI PubMed PMC
24. Amehri, W.; Zheng, G.; Kruszewski, A. FEM-based exterior workspace boundary estimation for soft robots via optimization. *IEEE. Robot. Autom. Lett.* **2022**, *7*, 3672-8. DOI

25. Schegg, P.; Duriez, C. Review on generic methods for mechanical modeling, simulation and control of soft robots. *PLoS. One.* **2022**, *17*, e0251059. DOI PubMed PMC
26. Wang, T.; Zhang, Y.; Zhu, Y.; Zhu, S. A computationally efficient dynamical model of fluidic soft actuators and its experimental verification. *Mechatronics* **2019**, *58*, 1-8. DOI
27. Peng, Y.; Sakai, Y.; Funabora, Y.; Yokoe, K.; Aoyama, T.; Doki, S. Funabot-Sleeve: a wearable device employing McKibben artificial muscles for haptic sensation in the forearm. *IEEE. Robot. Autom. Lett.* **2025**, *10*, 1944-51. DOI
28. Liew, A.; Gardner, L.; Block, P. Moment-curvature-thrust relationships for beam-columns. *Structures* **2017**, *11*, 146-54. DOI
29. Marsden, J.; Scheurle, J. The reduced Euler-Lagrange equations. In: Enos M, editor. Dynamics and control of mechanical systems: the falling cat and related problems. Providence: American Mathematical Society; 1993. pp. 139-64. https://www.semanticscholar.org/paper/The-Reduced-Euler-Lagrange-Equations-Marsden-Scheurle/cd941c78b9e22944a3e2afcba433ca021e401fa7. (accessed 2026-06-12).
30. Uppalapati, N. K.; Krishnan, G. Design and modeling of soft continuum manipulators using parallel asymmetric combination of fiber-reinforced elastomers. *J. Mech. Robot.* **2021**, *13*, 011010. DOI
31. Bartholdt, M.; Wiese, M.; Schappler, M.; Spindeldreier, S.; Raatz, A. A parameter identification method for static cosserat rod models: application to soft material actuators with exteroceptive sensors. In *2021 IEEE/RSJ International Conference on Intelligent Robots and Systems (IROS)*, Prague, Czech Republic, Sep 27 - Oct 01, 2021. IEEE; 2021. pp. 624-31. DOI